Engineering Geology 193 (2015) 276–287

Contents lists available at ScienceDirect

Engineering Geology

journal homepage: www.elsevier.com/locate/enggeo

Groundwater and earthquakes: Screening analysis for slope stability

Hugo A. Loáiciga

Department of Geography, University of California, Santa Barbara, CA 93106, United States

ARTICLE INFO

Article history:
Received 16 December 2014
Received in revised form 5 March 2015
Accepted 26 April 2015
Available online 29 April 2015

Keywords:
Slope stability
Groundwater
Earthquakes
Shear strength
Factor of safety
Seismic coefficient
Yield acceleration
Lateral spread displacement
Vertical reconsolidation

ABSTRACT

Groundwater is a factor behind the occurrence of landslides, and so is the action of seismic shaking in sloping terrain. This paper presents closed-form expressions for the factor of safety and yield coefficient of slopes subjected simultaneously to seismic forces and variable groundwater conditions. Two failure modes of natural slopes are considered in this work, namely, long slope with phreatic surface parallel to the ground surface and slope with emerging phreatic surface. For these failure modes, the factor of safety and yield coefficient are determined for various conditions of drainage using effective-stress analysis and total-stress analysis. The effect of soil strength reduction by seismic loading is accounted for in the derived factors of safety and yield coefficients. The specification of the lateral seismic coefficient for equivalent seismic loading relies on recent advances in geotechnical earthquake engineering and seismic engineering geology. The role of liquefaction and clay softening is introduced in the analysis of seismic slope stability and slope deformation considering variable groundwater conditions. Several examples illustrate the application of the methods herein presented.

1. Introduction

1.1. Landslide hazards

Landslides (the movement of a mass of debris, earth, or rock down a slope (Cruden and Varnes, 1996)) are perennial hazards that cause losses of life and property. Landslides are frequently associated with saturation of soils on slopes, which increases the weight of soils and reduces the effective stress (see, for example, Cedegreen, 1989; Anderson and Sitar, 1995; Iverson, 2000; Wang and Sassa, 2001; Duncan and Wright, 2005; Loáiciga, 2005). Another important cause of landslides is seismic shaking. In this case, the forces exerted on a slope produce stresses that exceed the strength of soils and rocks. Several authors have reported studies quantifying the linkages between earthquakes and landslides (see, for example, Seed, 1967, 1968; Keefer, 1984; Kramer, 1996; Jibson and Keefer, 1993; Evans and Bent, 2004; Harp et al., 2011; Jibson, 2011; Schulz et al., 2012). Landslide hazard mapping with geographic information systems (GIS) has advanced our capability to identify areas vulnerable to slope failure (Miller and Sias, 1998; Chacón et al., 2006).

In many instances slope failures are not due to natural phenomena, such as soil saturation or earthquakes, but to human actions. Among these, a common one is the removal of lateral support at the toe of slopes and the removal of vegetation that induces recharge to groundwater in sloping terrain (Gray and Megahan, 1981; Swanston et al., 1988; Miller and Sias, 1998; Brien and Reid, 2008).

1.2. Basic kinematics of landslides and paper's objectives

The mechanics of simultaneous earthquake loading and groundwater influences on slope stability are well elucidated by extending Newmark's (1965) classic analysis of the yield acceleration associated with a rotational slide with circular failure surface (A–B) of radius R centered at O, as depicted in Fig. 1. The sliding mass has weight W acting through its center of gravity (c.g.). All forces are expressed per unit length of the sliding mass perpendicular to the plane of Fig. 1. The effect of earthquake loading is captured through an equivalent, lateral (horizontal), force ($k_h \cdot W$) that passes through the center of gravity of the slice, where k_h is the seismic coefficient. The approach of replacing dynamic earthquake forces with an equivalent force $k_h \cdot W$ is referred to as pseudostatic analysis (Kramer, 1996). The seismic force is not horizontal, in actuality, as has been shown elsewhere (see Towhata, 2008, for example). However, it is common practice to specify the equivalent seismic force acting horizontally in the downslope direction when using the pseudostatic approach (Kramer, 1996; Stewart et al., 2003; Towhata, 2008).

The sliding mass shown in Fig. 1 experiences reaction forces N and groundwater forces U caused by pore pressure on the failure surface, and a resistance force S with moment arm R that acts in the direction opposing the direction of sliding. s_q denotes the dynamic shear strength

E-mail address: Hugo.Loaiciga@ucsb.edu.

http://dx.doi.org/10.1016/j.enggeo.2015.04.027
0013-7952/

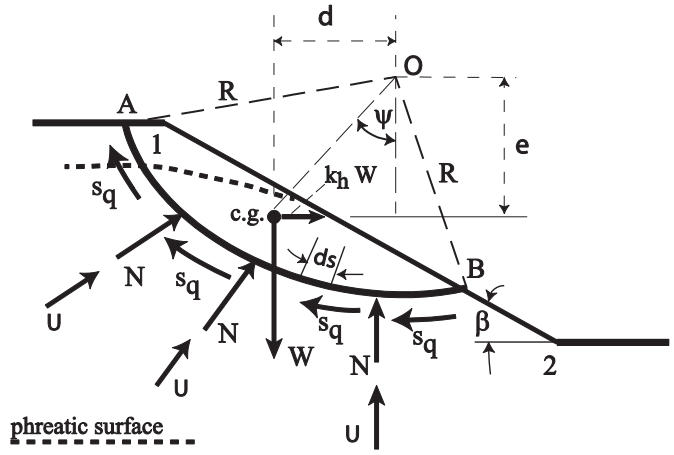

Fig. 1. Cross-sectional view of a rotational slide with key forces acting on the sliding mass.

(variable, in general, on the failure surface). R is the moment arm of the force S.

Equilibrium of moments can be used to calculate the factor of safety corresponding to the forces acting on the sliding mass of Fig. 1 (see, for example, Lambe and Whitman, 1979). The factor of safety is commonly used in screening or preliminary analyses of slope stability, prior to more involved stress-deformation analyses, if needed (Duncan, 1996; Griffiths and Lane, 1999; Griffiths and Marquez, 2007). The dynamic factor of safety, FS_q, corresponding to the sliding mass diagram of Fig. 1 is (with the index i denoting any of the shear strengths on the n arc lengths) can be shown to be:

$$FS_q = \frac{R \cdot \sum_{i=1}^{n} s_{qi} \cdot ds_i}{W \cdot d + (k_h \cdot W) \cdot e}. \quad (1)$$

Newmark's yield acceleration is obtained by setting the dynamic factor of safety equal to 1 in Eq. (1), and solving for the corresponding seismic coefficient, which, at limiting equilibrium, equals the yield coefficient, $k_y = a_y / g$, where a_y and g denote Newmark's yield acceleration and the acceleration of gravity, respectively. Assuming that the dynamic shear strengths (s_{qi}) equal the static shear strengths (s_{si}) on the failure surface, the following formula gives the yield acceleration corresponding to the conditions represented in Fig. 1:

$$a_y = g \cdot k_y = g \cdot (FS_{stat} - 1) \cdot \tan\psi \quad (2)$$

in which the static factor of safety (FS_{stat}) for the sliding mass is obtained from the dynamic factor of safety written in Eq. (1) by letting the dynamic shear strengths be equal to the static shear strengths and by setting the seismic coefficient $k_h = 0$. The term $tan\psi$ in Eq. (2) is replaced by $sin\psi$ when the seismic force has arbitrary orientation, giving rise to the well-known formula $a_y = g \cdot (FS_{stat} - 1) \cdot sin\psi$ (Newmark, 1965). There is downward displacement on the slope when the ground acceleration a exceeds the yield acceleration a_y, otherwise there is no displacement. Newmark's (1965) method is used to calculate total slope displacement by doubly integrating the $a - a_y$ difference with respect to time for all time intervals when the difference is positive and adding the integrated values.

The procedure leading to the dynamic factor of safety (1) and the yield acceleration (2) under the assumptions represented in Fig. 1 raises a number of issues that this paper addresses and attempts to provide answers to: (1) the effect of groundwater is captured by the weight of the sliding mass, since soil and rock increase their weights by saturation, and by possible changes in the pore pressure along the sliding surface; (2) the shape of the phreatic surface affects the factor of safety, as shown in this paper; (3) groundwater exerts net forces on the boundary of a slide's mass when there are tension cracks saturated with water (not shown in Fig. 1); (4) the effect of seismic forces is captured by the seismic coefficient, thus, its specification is of utmost importance to the outcomes of the proposed screening analysis for slope stability; (5) the nature of drainage in soils subjected to seismic shaking varies depending on the soils' hydraulic conductivities; (6) seismic loading is known to reduce the shear strength of soils, so the question arises as to what shear strength to use in the proposed screening analysis for slope stability; (7) liquefaction affects slope deformation, and variable groundwater conditions play a key role in this respect. This paper's innovation and contribution reside on providing a methodology for addressing issues (1) through (7) considering the simultaneous actions of earthquakes and variable groundwater conditions and relying on recent advances in geotechnical earthquake engineering and seismic engineering geology. Various formulas for the factor of safety and the yield coefficient are developed for common slope-failure modes (long slope with phreatic surface parallel to the ground surface and slope with emerging phreatic surface). These formulas incorporate the effect of liquefaction and clay softening and have practical value in conducting screening analyses of slope failure to assess slope-stability hazards. This paper does not cover reinforced or buttressed slopes, nor loads imposed by facilities constructed on a slope (see Stark and Poeppel, 1994; Koerner, 2012).

2. Seismic hazard and the seismic coefficient

Section 1 has shown how the seismic coefficient enters the stability and deformation analyses of slopes. Many authors have recommended values of the seismic coefficient, sometimes accounting for earthquake magnitude or maximal horizontal ground acceleration (Terzaghi, 1950; Marcuson, 1981; Seed, 1966, 1979; Hynes-Griffin and Franklin, 1984; Stewart et al., 2003; Towhata, 2008). Reported values range from as low as 0.05 for mild earthquakes to 0.50 for catastrophic ones. The method by Stewart et al. (2003) is used by many engineering geologists and geotechnical engineers in California (California Geological Society, 2008), a developed region with highly variable climate and threatened by seismicity (Keller and Loáiciga, 1993). It expresses the seismic coefficient as the product of a factor f_h times the normalized maximal horizontal acceleration on firm rock (MHA_r/g), $k_h = f_h \cdot MHA_r/g$. The factor f_h is a function of the nonlinear response of site soils overlying firm rock to seismic shaking, the slope displacement, the duration of strong shaking, the earthquake (moment) magnitude (M), and the distance (r) between the slope site and the source of the earthquake (California Geological Society, 2008). Fig. 2 shows the seismic coefficient as a function of the MHA_r/g calculated with the method of Stewart et al. (2003) (see also California Geological Society, 2008) for allowed slope deformations (d) equal to 5 and 15 cm, when the

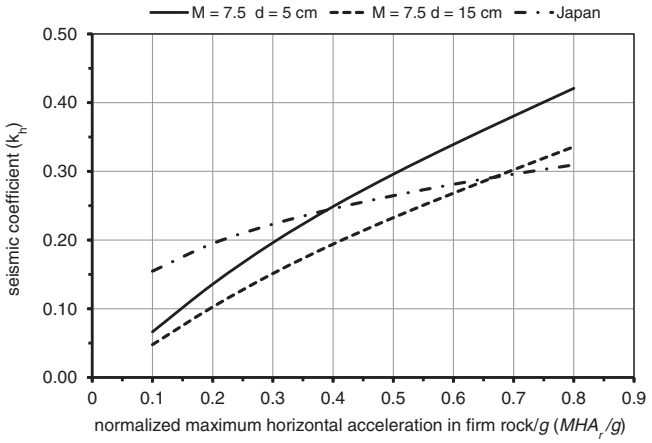

Fig. 2. The seismic coefficient (k_h) as a function of key parameters using the method of Stewart et al. (2003) and the formula reported by Noda et al. (1975) and Towhata (2008), Japan.

earthquake magnitude and the distance from the slope site to the earthquake source are $M = 7.5$ and $r = 30$ km, respectively. In addition, Fig. 2 depicts the seismic coefficient as reported by Noda et al. (1975) and Towhata (2008) in which k_h is a function of the maximal (horizontal) ground acceleration at ground level (MHA), $k_h = (MHA/g)^{1/3} / 3$. It is evident in Fig. 2 that the smaller allowable deformation (5 cm) results in larger (or more conservative) values of the seismic coefficient, other variables being equal, when using the Stewart et al. (2003) method. The formula reported by Noda et al. (1975) and Towhata (2008) produces a seismic coefficient that is larger (or smaller) than that calculated with the Stewart et al. (2003) method at low (or high) values of the ground acceleration. Seismic hazard maps depicting the MHA_r have been compiled by the United States Geological Survey (Petersen et al., 2008) for various probability scenarios in the United States.

3. Specification of the shear strength of soils used in the screening analysis of seismic slope stability

The specification of the shear strength is of utmost importance in the screening analysis of seismic slope stability. This is so because the shear strength that soils mobilize during earthquake shaking, or dynamic shear strength, controls the stability of slopes during earthquakes. The earthquake-related phenomena of liquefaction (Mogami and Kubu, 1953; Kramer, 1996) and clay softening (loss of shear strength and large deformations experienced by saturated clays and elastic silts subjected to cyclic loading, Idriss and Boulanger, 2008) also affect slope stability, and they are included in this paper's analysis of slope stability.

3.1. Approaches to the specification of the shear strength of soils under earthquake loading

Concerning nonliquefiable soils, Maksidi and Seed (1978) recommended the use of 0.80 the (monotonic or static) undrained shear strength (s_u) as a proxy to the dynamic yield strength for use with total-stress analysis of seismic slope stability. This recommendation was made for soils that exhibit small increases in pore pressure during cyclic, undrained, loading, such as clayey materials, dry or partially saturated cohesionless soils, or very dense saturated cohesionless materials. The use of 0.80 times the (static) undrained shear strength as an equivalent dynamic shear strength has been reported for saturated clays and elastic silts softened by earthquake shaking (Idriss and Boulanger, 2008).

Hynes-Griffin and Franklin (1984) recommended a variation of the Maksidi and Seed (1978) dynamic yield strength. Specifically, the former authors recommended the following seismic coefficient and shear strengths when the moment magnitude of earthquakes is less than 8.0: (a) use a seismic coefficient k_h equal to one half the mapped maximal horizontal acceleration (expressed as a fraction of g) in firm rock; (b) use 0.80 of the consolidated drained (CD) triaxial compressive shear strength for pervious soils at low confining stress, effective-stress analysis; (c) use 0.80 of the consolidated undrained (CU) triaxial compressive shear strength, total-stress analysis, for pervious soils at high confining stress; and (d) use of the 0.80 of the CU triaxial compressive shear strength, total-stress analysis, for clays.

Blake et al. (2002) made recommendations for shear strength that attempted to strike a balance between the performance of slopes under seismic loads and the cost of taking measures to ensure an adequate performance. In the case of coarse-grained, saturated, alluvium, for example, Blake et al. (2002) recommended using consolidated drained direct shear strength (DS) or consolidated drained (CD) triaxial compressive shear strength, effective-stress analysis, if the soil is nonliquefiable, or using the undrained residual strength, total-stress analysis, if the soil is liquefiable. Another example of Blake et al.'s (2012) recommendations was using unconsolidated undrained (UU) or CU shear strength, total-stress analysis, with fine-grained, saturated and soft, alluvium, applying judgment to choose between peak strength or residual strength. The previous survey of approaches for specifying shear strength of soils in screening analysis of seismic slope stability reveals a wide variance in the use of shear strengths. This is remarkable, given that seismic forces act rapidly on slope soils, which, if saturated, are likely to experience undrained loading conditions in all but the most pervious soils (Lambe and Whitman, 1979).

3.2. The residual shear strength in liquefied sands

The residual shear strength (s_r) is used in slopes whose soils liquefy by seismic loading. Seed and Harder (1990) reported correlations between a normalized standard penetration (SPT) resistance $(N_1)_{60cs-rs}$ in clean sands and their residual shear strength. The residual shear strength proposed by the latter authors is obtained by inferring slope geometry to its pre-failure shape at sites where landslides occurred and then calculating (or, in the jargon, "back-calculating") the (residual) strength along the failure surface that would produce limit equilibrium (factor of safety equal to 1). Stark and Mesri (1992) presented a correlation between the ratio of the residual strength of cohesionless soils (s_r) to the vertical effective stress on the failure surface (σ'_{v0}), or normalized residual strength (s_r/σ'_{v0}), and a normalized SPT resistance in clean sands ($(N_1)_{60cs-rs}$), where $(N_1)_{60cs-rs}$ was obtained with corrections for fines content that differ from those used by Seed and Harder (1990). Idriss and Boulanger (2008) reported correlations between (i) the normalized residual shear strength (s_r/σ'_{v0}) and a normalized SPT resistance of clean sands ($(N_1)_{60cs-rs}$, the latter obtained identically as in Seed and Harder, 1990), and (ii) the normalized residual strength and the post-earthquake cone penetration (CPT) resistance of clean sands.

3.3. Determination of the liquefaction potential of saturated sands on sloping terrain

The determination of the liquefaction potential of slope soils is key to the specification of the appropriate shear strength in the screening method for seismic slope stability. Liquefaction also affects slope deformation, and variable groundwater conditions are relevant in this respect. The simplified procedure for evaluating liquefaction potential (Seed and Idriss, 1971; Youd et al., 2001) is widely used, and herein adopted. Updated formulas for the simplified approach were published by Idriss and Boulanger (2008). The simplified approach makes an evaluation of liquefaction potential based on the factor of safety against liquefaction, FS_{liq}. Two key variables that enter the FS_{liq} are the seismic stress ratio (CSR) and the seismic resistance ratio (CRR). The CSR is a normalized measure of the stress caused by an earthquake with maximal ground acceleration MHA. It is the ratio of the average cyclic stress to the vertical effective stress (σ'_{v0}). The CRR is a measure of the capacity of saturated sand to resist liquefaction. The CSR is given by the formula:

$$CSR = \frac{0.65 \cdot \left(\frac{MHA}{g}\right) \cdot \sigma_{v0} \cdot r_d}{\sigma'_{v0}} \tag{3}$$

in which MHA represents the maximal horizontal acceleration at ground surface, σ_{v0} and σ'_{v0} denote the vertical total and vertical effective stresses, respectively, at a specified depth below the ground surface; r_d is a stress-reduction coefficient that accounts for the flexibility of the soil profile (Youd et al., 2001; Idriss and Boulanger, 2008).

The CRR is expressed in terms of empirical correlations, in which the dependent variable is the normalized SPT resistance $(N_1)_{60}$, or a normalized CPT tip resistance (q_{c1N}), or a corrected shear-wave velocity (Youd et al., 2001; Idriss and Boulanger, 2008). The CRR depends on the moment magnitude of the earthquake (M), the vertical effective stress (σ'_{v0}), the static shear stress ratio (α), and the fines content of a soil.

The static shear stress ratio equals the static shear stress at a point on the failure surface of a slope (τ_{stat}) divided by the vertical effective stress at the same point ($\alpha = \tau_{stat}/\sigma'_{v0}$). The correlations for the CRR have been developed for a reference condition ($CRR_{M=7.5;\ \sigma'_{v0}=1\ atm;\ \alpha=0}$) in which the earthquake magnitude equals 7.5, the vertical effective stress equals one atmosphere of pressure ($\sigma'_{v0} = 101.325$ kPa), the terrain is level ($\alpha = 0$), and the fines content of sand is equal to or less than 5% (this defines the "clean-sand" condition). The CRR for earthquakes of arbitrary magnitude, arbitrary vertical effective stress, on sloping terrain ($\alpha > 0$) ($CRR_{M;\ \sigma'_{v0};\ \alpha}$) is obtained by multiplying the reference CRR by a moment scaling factor (*MSF*, which equals 1 when the earthquake magnitude is 7.5), a geostatic correction factor (K_σ), and a static stress ratio factor ($K\alpha$), as follows:

$$CRR_{M;\ \sigma'_{v0};\ \alpha} = CRR_{M=7.5;\ \sigma'_{v0}=1\ atm;\ \alpha=0} \cdot K_\sigma \cdot K_\alpha \cdot MSF. \quad (4)$$

Idriss and Boulanger (2008) reported updated expressions for all the variables shown on the right-hand side of Eq. (4). The factor of safety against liquefaction (FS_{liq}) is then:

$$FS_{liq} = \frac{CRR_{M;\ \sigma'_{v0};\ \alpha}}{CSR} = \frac{CRR_{M=7.5;\ \sigma'_{v0}=1\ atm;\ \alpha=0} \cdot K_\sigma \cdot K_\alpha \cdot MSF}{\left(0.65 \cdot \left(\frac{MHA}{g}\right) \cdot \sigma_{v0} \cdot r_d}{\sigma'_{v0}}\right)}. \quad (5)$$

If the factor of safety against liquefaction is equal to or less than 1 then the sand is liquefiable per the simplified procedure embodied by Eq. (5). In this case, the use of the residual shear strength discussed in the previous subsection is appropriate in the screening analysis of seismic slope stability. Groundwater conditions affect the CSR and the factors K_σ and $K\alpha$ that appear in Eq. (5). Applications of Eq. (5) in slope stability and deformation analyses are presented in the Results section.

3.4. The dynamic shear resistance associated with clay softening

The phenomenon of clay softening in saturated clays and elastic silts subjected to cyclic loading is reflected in the form of large soil deformations and reduced shear strength. Clay softening has been defined as the onset of shear strains (δ) equal to or larger than 3% (Idriss and Boulanger, 2008). The factor of safety against clay softening, $FS_{\delta = 3\ \%}$ equals the ratio of the cyclic resistance ratio for arbitrary earthquake (moment) magnitude (M) in sloping terrain ($CRR_{M,\alpha}$) divided by the cyclic stress ratio (CSR) introduced in Eq. (3).

The slope effect on clay softening is captured by means of the static shear stress ratio (α) defined in the previous section dealing with dynamic liquefaction. In a manner analogous to the evaluation of liquefaction potential, the $CRR_{M,\alpha}$ is obtained by multiplying the reference CRR for earthquakes of magnitude 7.5 on level terrain, $CRR_{M\ =\ 7.5,\ \alpha\ =\ 0}$, times a magnitude scaling factor for clay softening (MSF_{CS}, which equals 1 when the earthquake magnitude is 7.5) and times a stress ratio factor $K_{\alpha,CS}$:

$$CRR_{M,\ \alpha} = CRR_{M=7.5,\ \alpha=0} \cdot MSF_{CS} \cdot K_{\alpha,\ CS} = \frac{0.80 \cdot s_u}{\sigma'_{v0}} \cdot MSF_{CS} \cdot K_{\alpha,\ CS}. \quad (6)$$

Notice in Eq. (6) that the reference CRR is equal to a dynamic strength $0.80 \cdot s_u$, where s_u denotes the static undrained shear strength, divided by the vertical effective stress at a point on the failure surface. Idriss and Boulanger (2008) provide formulas for MSF_{CS} and $K_{\alpha,\ CS}$. $K_{\alpha,\ CS}$ equals 1 when the terrain is level. See the Results section for an example. The safety factor against clay softening is then:

$$FS_{\delta=3\%} = \frac{CRR_{M,\ \alpha}}{CSR} = \frac{\frac{0.80 \cdot s_u}{\sigma'_{v0}} \cdot MSF_{CS} \cdot K_{\alpha,\ CS}}{\left(0.65 \frac{MHA}{g} \cdot \sigma_{v0} \cdot r_d}{\sigma'_{v0}}\right)} = \frac{1.23 \cdot MSF_{CS} \cdot K_{\alpha,\ CS}}{\frac{MHA}{g} \cdot \sigma_{v0} \cdot r_d} \quad (7)$$

in which all terms have been previously defined. In the proposed screening analysis of seismic slope stability one would calculate the factor of safety against clays softening. If the factor of safety exceeds 1, use the full static undrained shear strength in the analysis of seismic slope stability. Otherwise, use 0.80 the undrained shear strength as an equivalent dynamic shear strength in the seismic slope stability analysis. An example of the impact of groundwater conditions on clay softening is presented in the Results section.

4. Factors of safety for slope stability and corresponding yield accelerations

This section develops and presents the closed-form expressions for the factor of safety (FS) and yield coefficient ($k_y = a_y/g$) of slopes affected by groundwater and undrained seimic loading. Results pertaining to effective stress (drained) analysis of slope stability are presented for completeness.

4.1. Translational slides on long slopes: phreatic surface parallel to slope

Fig. 3 shows the geometry and variables that enter the stability analysis of a long ("infinite" in the geotechnical jargon) slope with phreatic

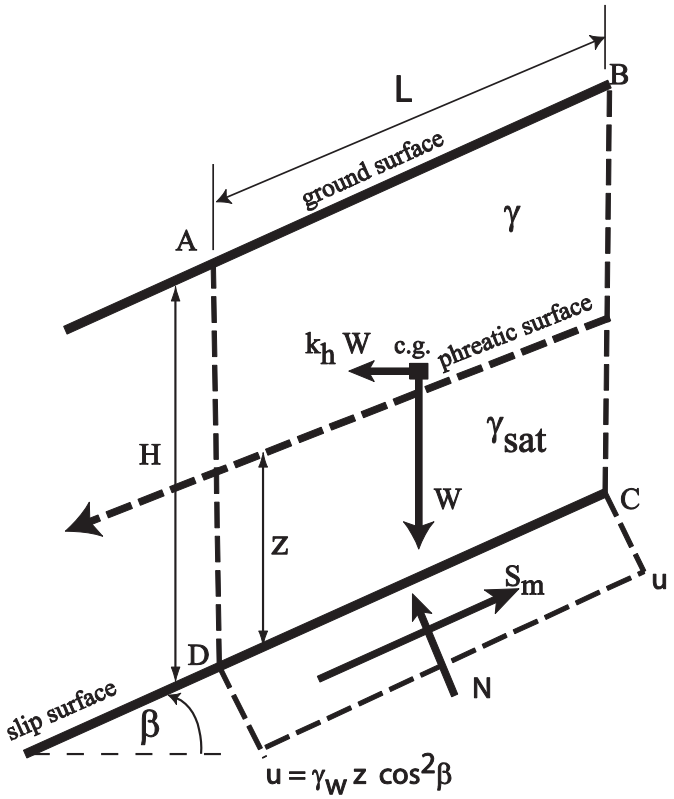

Fig. 3. Geometry and variables that enter in the stability analysis of a long slope with phreatic surface parallel to the slope. u denotes the steady-state pore pressure on the slip surface. Elevation view.

surface parallel to the sloping (ground) surface. A translational slide on a long slope is such that the thickness of the sliding mass (H) is much smaller than its length (L). The analysis of the stability of long slopes is generalized in this work to include seismic forces. Empirical evidence indicates that the thickness of translational slides is commonly less than $H = 3$ m(Cruden and Varnes, 1996). In reference to Fig. 3, W and z denote the weight of the sliding mass (enclosed within the parallelogram ABCD) and the height of saturation above the slip surface, respectively; N, S_m, and u denote the reaction normal to the slip surface, the mobilized shear resistance force needed to maintain equilibrium (Bishop, 1955; Bishop and Morgenstern, 1960), and the pore pressure, respectively, all acting on the slip surface; γ and γ_{sat} are the unsaturated and saturated unit weights of the sliding mass, respectively. The steady-state pore pressure corresponding to a phreatic surface parallel to the ground surface generates a (steady-state) pressure force $= U = u \cdot L = \gamma_w z \cos^2\beta \cdot L$ acting normal to the slip surface, where γ_w denotes the unit weight of water (9.81 kN/m^3). The steady-state pressure forces acting on the vertical sides AD and BC cancel each other. All forces are per unit width of slope perpendicular to the plane of the drawing (in this case, of Fig. 3). The steady-state pressure most likely differs from the actual pressure attained during seismic loading. The dynamic pressure is unknown, however, and, therefore, the effective-stress analysis uses its steady-state value as an approximation. The difficulty of specifying a pore pressure on the slip surface is avoided when total stress analysis is used, as shown below. The effect of saturation on the sliding mass is reflected on its weight and on the pressure force U. The weight of the sliding mass depends on the average unit weight, which is $\gamma_{avg} = (\gamma(H - z) + \gamma_{sat} z)/H$. As the depth of saturation (z) rises, the sliding mass becomes heavier and the frictional resistance of the mobilized shear resistance force is diminished. In addition, the pseudostatic driving force ($k_h \cdot W$) increases with increasing weight of the sliding mass.

Using effective stress analysis, wherein c' and ϕ' denote the effective stress cohesion and angle of internal friction on the slip surface, respectively, it follows that the mobilized shear resistance force equals $S_m = (c' \cdot L/FS) + \tan\phi' \cdot (N - U)/FS$, in which FS denotes the factor of safety on the slip surface, and the effective reaction N–U must be positive from physical plausibility requirement. The equilibrium of forces parallel and normal to the slip surface in Fig. 3 produces the following factor of safety in the case of effective stress analysis:

$$FS = \frac{c'}{\gamma_{avg} H}\left[\frac{1}{\cos^2\beta \cdot (k_h + \tan\beta)}\right] + \left[\frac{1 - k_h \tan\beta - \dfrac{\gamma_w z}{\gamma_{avg} H}}{(k_h + \tan\beta)}\right]\tan\phi' . \quad (8)$$

The first term on the right-hand side of Eq. (8) measures the effect of cohesion on slope stability, whereas the second term reflects the contribution of internal friction to slope stability. It is evident in Eq. (8) that augmenting the seismic coefficient k_h diminishes the factor of safety. It follows from Eq. (8) that increasing the saturation of the sliding mass reduces the factor of safety, also, because the average unit weight (γ_{avg}) increases with increasing depth of saturated thickness (z), thus making the slope less stable when the phreatic surface rises.

Setting the factor of safety in Eq. (8) equal to one and letting $k_h = k_y \equiv a_y/g$ one solves for the yield coefficient (k_y, for downslope motion):

$$k_y = \frac{c'}{\gamma_{avg} H} \cdot \frac{1}{\cos^2\beta \cdot (1 + \tan\beta \cdot \tan\phi')} + \frac{\tan\phi' \cdot \left(1 - \dfrac{\gamma_w z}{\gamma_{avg} H}\right) - \tan\beta}{1 + \tan\beta \cdot \tan\phi'} . \quad (9)$$

Increasing the saturation of the sliding mass (that is, larger z) decreases the yield coefficient in Eq. (9). This means that larger slope deformations are likely when the weight of the sliding mass increases with increasing groundwater depth.

A case of special interest is that of cohesionless soils ($c' = 0$), in which case the corresponding factor of safety and yield coefficient are derived by letting $c' = 0$ in Eqs. (8) and (9), respectively. The case of a cohesionless, dry, soil is handled by letting $c' = 0$ and $z = 0$ in Eqs. (8) and (9). In this instance, non-negativity of the yield coefficient commands that $\phi' > \beta$. Eq. (8) subsumes the static factor of safety on a dry slope as a special case: letting $c' = 0, z = 0, k_h = 0$ in Eq. (8) establishes that $FS_{stat} = \tan\phi'/\tan\beta$, where $\phi' > \beta$ is required for slope stability in this simplest of cases. Eqs. (8) and (9) apply to pervious slope soils capable of draining during seismic loading. It is common practice to estimate the strength coefficients c' and ϕ' from standardized test methods, such as the direct shear test and the consolidated drained triaxial compression test.

The use of total stress in the analysis of the stability of a long slope bypasses the need of specifying the pore pressure on the slip surface, which is set equal to zero in this type of analysis. Water pressures exerted on other external boundaries, if they exist, must be considered, however. Total stress analysis relies on the total-stress cohesion (c_T) and angle of friction (ϕ_T), which can be estimated from consolidated undrained tests, when applicable. Force equilibrium applied with the total stress analysis produces the following expressions for the factor of safety and the yield coefficient:

$$FS = \frac{c_T}{\gamma_{avg} H} \cdot \left[\frac{1}{\cos^2\beta \cdot [k_h + \tan\beta]}\right] + \left[\frac{1 - k_h \tan\beta}{k_h + \tan\beta}\right] \cdot \tan\phi_T \quad (10)$$

$$k_y = \frac{c_T}{\gamma_{avg} H} \cdot \frac{1}{\cos^2\beta \cdot (1 + \tan\beta \cdot \tan\phi_T)} + \frac{\tan\phi_T - \tan\beta}{1 + \tan\beta \cdot \tan\phi_T} . \quad (11)$$

Eq. (10) proves that increases in the unit weight of the sliding mass and in the seismic coefficient reduce the factor of safety, making the slope less stable when the phreatic surface rises. The factor of safety in Eq. (10) decreases with increasing value of the seismic coefficient. The yield coefficient in Eq. (11) decreases with increasing saturation thickness (z) in the sliding mass. This condition exacerbates slope deformation.

An important variation of total stress analysis is the $\phi_T = 0$ case, which applies to a saturated soil that is sheared undrained (i.e., unconsolidated undrained or UU shearing). The $\phi_T = 0$ analysis leads to substantial simplifications in the analysis of slope stability because (i) pore pressures are not specified on the slip surface, and (ii) the shear strength of a soil is expressed by one parameter, the undrained shear strength (s_u). It was stated in Section 3 that several authors recommend the use of a dynamic shear strength (s_q) equal to 0.80 s_u when clay softening occurs during seismic loading. If sands are liquefied, then a dynamic shear strength equal to the residual shear strength (s_r) should be used instead in the $\phi_T = 0$ total-stress analysis. Force equilibrium leads to the following results of slope stability when applying the $\phi_T = 0$ total-stress analysis. In the next two equations the dynamic shear strength symbol s_q can be replaced by the undrained shear strength s_u, the residual shear strength s_r, or the clay-softened strength 0.80 s_u depending of field conditions and the analyst's judgment:

$$FS = \frac{s_q}{\gamma_{avg} H} \cdot \frac{1}{\cos^2\beta \cdot [k_h + \tan\beta]} \quad (12)$$

$$k_y = \frac{s_q}{\gamma_{avg} H} \cdot \frac{1}{\cos^2\beta} - \tan\beta . \quad (13)$$

Eq. (12) shows that in the $\phi_T = 0$ case the factor of safety (i) decreases when the saturation thickness (z) increases (because the average unit weight increases), and (ii) it decreases when the seismic force increases (that is, when k_h increases). The yield coefficient in Eq. (13) decreases with increasing average unit weight of the sliding mass, that is, with rising phreatic surface. The Results section shows that the factor of safety and the yield coefficient decrease with increasing

slope angle (β) up to a value of the slope angle at which the yield coefficient becomes equal to zero (see Fig. 11).

4.2. Translational slides on long slopes: phreatic surface emerging from the slope

Fig. 4 depicts the variables that enter the stability analysis of long slopes with emerging phreatic surface. The emergence of groundwater on a slope manifests itself visually in the form of springs or other forms of surface runoff on the surface of a slope.

The analysis of the stability of long slopes with emerging phreatic surface is generalized in this work to include seismic forces. All the variables displayed in Fig. 4 were defined when discussing Fig. 3, except for the angle φ that the phreatic surface forms with the horizontal. The variable u denotes the pore pressure acting normal to the slip surface. Steady-state pressure forces acting on the vertical sides AD and BC cancel each other. Starting with effective-stress analysis of the slope shown in Fig. 4, force equilibrium of the parallelogram ABCD leads to the following factor of safety:

$$FS = \frac{c'}{\gamma_{sat} H} \cdot \frac{1}{\cos^2\beta \cdot [k_h + \tan\beta]} + \frac{1 - k_h \tan\beta - \dfrac{u}{\gamma_{sat} H \cos^2\beta}}{k_h + \tan\beta} \tan\phi' \quad (14)$$

in which the steady-state pore pressure acting normal to the slip surface equals $u = \gamma_w H/(1 + \tan\beta \cdot \tan\varphi)$. The yield coefficient is as follows:

$$k_y = \frac{c'}{\gamma_{sat} H} \cdot \frac{1}{\cos^2\beta \cdot (1 + \tan\beta \cdot \tan\phi')} + \frac{\tan\phi' \cdot \left(1 - \dfrac{u}{\gamma_{sat} H \cos^2\beta}\right) - \tan\beta}{1 + \tan\beta \cdot \tan\phi'}. \quad (15)$$

Notice that the sliding mass (body of soil ABCD in Fig. 4) is fully saturated (its unit weight equals γ_{sat}). Secondly, the angle φ appears only in the pore pressure term u. In addition, it is evident in Eq. (14) that increasing the seismic coefficient decreases the factor of safety, and, thus, reduces the stability of a slope. Cohesionless conditions are readily derived from Eqs. (14) and (15) by setting $c' = 0$.

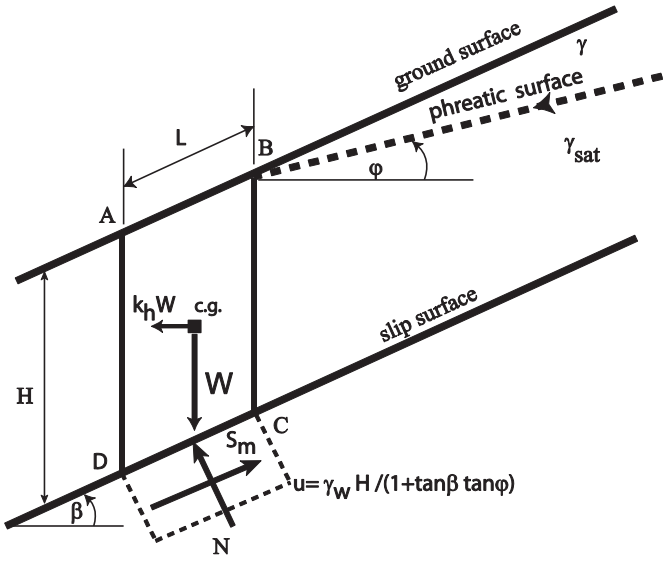

Fig. 4. Geometry and variables than enter the stability analysis of a long slope with emerging phreatic surface. u denotes the steady state pressure on the slip surface. Elevation view.

Total-stress stability analysis of the long slope with emerging phreatic surface relies on the total stress parameters c_T and ϕ_T and setting the pore pressure equal to zero on the slip surface. The total-stress factor of safety is:

$$FS = \frac{c_T}{\gamma_{sat} H} \cdot \frac{1}{\cos^2\beta \cdot [k_h + \tan\beta]} + \frac{1 - k_h \tan\beta}{k_h + \tan\beta} \cdot \tan\phi_T. \quad (16)$$

Eq. (16) indicates that the factor of safety decreases with increasing seismic coefficient. The total-stress yield coefficient is given by:

$$k_y = \frac{c_T}{\gamma_{sat} H} \cdot \frac{1}{\cos^2\beta \cdot (1 + \tan\beta \cdot \tan\phi_T)} + \frac{\tan\phi_T - \tan\beta}{1 + \tan\beta \cdot \tan\phi_T}. \quad (17)$$

Total-stress analysis of slope stability setting $\phi_T = 0$ (unconsolidated undrained conditions) is of utmost relevance in seismic slope stability analysis. Force equilibrium of the sliding mass ABCD in Fig. 4 leads to the following formulas for the factor of safety and yield coefficient of the case $\phi_T = 0$:

$$FS = \frac{s_q}{\gamma_{sat} H} \cdot \frac{1}{\cos^2\beta \cdot [k_h + \tan\beta]} \quad (18)$$

in which the dynamic shear strength symbol s_q can be replaced by the undrained shear strength s_u, the residual shear strength s_r, or the clay-softened strength 0.80 s_u depending on field conditions and the analyst's judgment. The factor of safety is clearly reduced by increasing the seismic coefficient in Eq. (18). Notice that the factor of safety in Eq. (18) (with unit weight γ_{sat}) differs from that of a phreatic surface parallel to the slope surface (Eq. (12), with unit weight γ_{avg}) only in the specification of the unit weight of the sliding mass. The yield coefficient is:

$$k_y = \frac{s_q}{\gamma_{sat} H} \cdot \frac{1}{\cos^2\beta} - \tan\beta \quad (19)$$

where all variables have been previously defined. Notice the similarity between the yield coefficient in Eq. (19) for the case of an emerging phreatic surface and that of the yield coefficient for the case of a parallel phreatic surface given in Eq. (13): they differ only by the specification of the unit weight of the sliding mass. The factor of safety in Eq. (18) and the yield coefficient in Eq. (19) decrease with increasing slope angle up to a value of the slope angle at which the yield coefficient becomes equal to zero. This behavior is analogous to the role that slope angle has on the seismic stability of long slopes with phreatic surface parallel to the slope surface (see Eqs. (12) and (13), and Fig. 11).

5. Effect of groundwater on the deformation of liquefied soils

This section highlights the effect of phreatic surface variations on (i) the lateral spread displacement, and (ii) the vertical reconsolidation of liquefied sands. Lateral spread is defined as the horizontal displacement at the ground surface caused by seismic shaking in terrain sloping to a free (or open) face. Two approaches to the quantification of lateral spread displacement in sloping terrain are entertained in this paper. The first one is based on empirical regression equations that relate measured lateral spread to several indicator variables. The second one is based on the integration of the calculated permanent maximal shear strains over the depth of liquefied soils to produce the lateral deformation at ground surface. Maximal shear strain is calculated using empirical formulas that relate shear strain in liquefied sand to in-situ measurable properties such as the standard penetration test (SPT) N value normalized to a clean-sand equivalent $(N_1)_{60cs}$, or the normalized cone penetration test (CPT) tip resistance normalized to a clean-sand equivalent (q_{c1Ncs}). Vertical reconsolidation is the settlement of the ground surface of liquefied soils caused by seismic shaking. Vertical reconsolidation is herein approached using empirical formulas that

relate the vertical deformation of liquefied sand to in-situ measurable properties such as the $(N_1)_{60cs}$ or q_{c1Ncs}.

5.1. The effect of groundwater on lateral spread displacement calculated using regression formula

The role of groundwater on lateral spread displacement (D_H) is illustrated with the regression equation presented by Youd et al. (2002), in which D_H in gently sloping terrain (in meters) is regressed on the following variables: M, the earthquake moment magnitude; R, the map distance from the site of spreading to the nearest bound of the seismic source; S, the slope of terrain (as a percentage); T_{15}, the cumulative thickness (in meters) of saturated granular layers with normalized SPT resistance $(N_1)_{60}$ less than 15; FC_{15}, the average fines content, expressed as a percentage, of the layers included in the calculation of T_{15}, in which fines are soil particles that pass the No. 200 standard sieve; $D50_{15}$, the average mean particle size (in mm) of the layers included in the calculation of T_{15}. The regression formula is as follows (Youd et al., 2012):

$$\begin{aligned} logD_H = {} & a_1 + b_1 M + c_1 logR^* + d_1\, R + \ e_1 \log S + f_1 logT_{15} \\ & + g_1 \log(100 - FC_{15}) + h_1 \log(D50_{15} + 0.1) \end{aligned} \tag{20}$$

in which a_1, b_1, c_1, d_1, e_1, f_1, g_1, and h_1 equal −16.213, 1.532, −1.406, −0.012, 0.338, 0.540, 3.413, and −0.795, respectively, and

$$R^* = R + 10^{0.89M - 5.64}. \tag{21}$$

Groundwater impacts the lateral spread displacement through the elevation of the phreatic surface (or "water table"), which determines the layers that are involved in the calculation of T_{15}, FC_{15}, and $D50_{15}$: a fully saturated soil profile includes all the underlying granular layers, thus leading to a potentially large lateral spread displacement. A deep phreatic surface, on the other hand, might avoid liquefaction altogether. One example of the impact of groundwater on lateral spread displacement is presented in the Results section.

5.2. The effect of groundwater on lateral ground deformation based on the integration of shear strain

A potential maximal lateral spread displacement, named lateral displacement index (LDI) by Zhang et al. (2004), is obtained by integrating the maximal shear strain, $\gamma_{max}(z)$, over the depth z of the soil profile:

$$LDI = \sum_{z=0}^{H} \gamma_{\max}(z) \Delta z. \tag{22}$$

The maximal shear strain γ_{max} as a function of depth z depends on (i) the stiffness of the granular soils expressed in terms of the SPT or CPT resistances or the relative densities, and (ii) the factor of safety against liquefaction (introduced in Eq. (5)) forgranular layers (Yoshimine et al., 2006). Only the formulas corresponding to the SPT resistance are presented in this paper. The calculation algorithm for Eq. (22) starts with the calculation of the factor F_γ and the limiting shear strain γ_{lim}. The latter two variables are calculated as follows when expressed in terms of the normalized SPT resistance $(N_1)_{60cs}$ in clean sands (Yoshimine et al., 2006):

$$F_\gamma = 0.032 + 0.69\sqrt{(N_1)_{60cs}} - 0.13\,(N_1)_{60cs} \qquad (N_1)_{60cs} \geq 7 \tag{23}$$

$$\gamma_{lim} = 1.859 \cdot \left(1.1 - \sqrt{\frac{(N_1)_{60cs}}{46}}\right)^3. \tag{24}$$

The normalized SPT resistance of clean sands in Eqs. (23) and (24) is as follows (Idriss and Boulanger, 2008):

$$(N_1)_{60cs} = (N_1)_{60} + \Delta(N_1)_{60} \tag{25}$$

$$\Delta(N_1)_{60} = e^{\left(1.63 + \frac{9.7}{FC + 0.01} - \left(\frac{15.7}{FC + 0.01}\right)^2\right)} \tag{26}$$

where FC denotes the fines content (in percent) at depth z. Thereafter, one of the following three equations is chosen to calculate the maximal shear strain at a depth z (Yoshimine et al., 2006):

$$\gamma_{max}(z) = 0 \ \text{ if } \ FS_{liq} \geq 2 \tag{27}$$

$$\gamma_{max}(z) = smaller\ of \left[\gamma_{lim}; 0.035(2 - FS_{liq}) \cdot \left(\frac{1 - F_\gamma}{FS_{liq} - F_\gamma}\right)\right] \ \text{ if } \ F_\gamma < FS_{liq} < 2 \tag{28}$$

$$\gamma_{max}(z) = \gamma_{lim} \ \text{ if } \ FS_{liq} \leq F_\gamma. \tag{29}$$

The effect of the position of the phreatic surface on the maximal shear strain is reflected on the value of the factor of safety against liquefaction (FS_{liq}, see Eq. (5)), which establishes a connection between groundwater conditions on site and the LDI. Once the maximal shear strain (γ_{maxi}) is calculated in layers of liquefied sand, each of thickness Δz_i, the LDI given by Eq. (22) is approximated by integrating numerically:

$$LDI \cong \sum\nolimits_i \Delta z_i\ \gamma_{maxi}\ . \tag{30}$$

The Results section presents an example of the calculation of the lateral displacement index.

5.3. The effect of groundwater on vertical reconsolidation based on the integration of vertical strain

Vertical (one-dimensional) reconsolidation of liquefied sands, S_v, is herein calculated with the method of Yoshimine et al. (2006), in which the vertical strain (ε_v) of liquefied layers is related to the maximal shear strain (γ_{max}), introduced in the previous subsection, and to the equivalent SPT resistance in clean sand ($(N_1)_{60cs}$):

$$\varepsilon_v = 1.5(\ e^{-0.369\ (N_1)_{60cs}}\ ) \cdot \text{smaller of } [0.08, \gamma_{\max}\ ] \tag{31}$$

$(N_1)_{60cs}$ is calculated with Eqs. (25)–(26), and γ_{max} is calculated with Eq. (27), or (28), or (29), as the case might be. Once the vertical strains (ε_{vi}) in liquefied layers of thickness Δz_i are calculated, the vertical reconsolidation is approximated as follows:

$$S_v \cong \sum\nolimits_i \Delta z_i\ \varepsilon_{vi}. \tag{32}$$

The vertical strain depends on the shear strain, which, as stated in Eqs. (27)–(29), depends on the factor of safety against liquefaction, which in turn, depends on groundwater conditions. This chain of relations establishes a connection between groundwater conditions and vertical reconsolidation, which is illustrated by example in the Results section. An earlier method to calculate the vertical reconsolidation of liquefied sand was presented by Tokimatsu and Bolton Seed (1987).

6. Results

This section presents a few examples of the key results of this paper.

6.1. Long slopes: parallel phreatic surface and emerging phreatic surface

The first example deals with effective-stress analysis of the stability of a long slope with phreatic surface parallel to the slope surface, whose geometry is portrayed in Fig. 3. The chosen slope parameter values are as follows: $c' = 0$, $\phi' = 35°$, slope thickness $H = 3$ m, $\gamma_{sat} = 20.42$ kN/m^3, γ (unsaturated) $= 15.71$ kN/m^3, $\gamma_w = 9.81$ kN/m^3, slope angle $\beta = 12°$. Fig. 5 graphs the calculated factor of safety for (i) static case (there is no seismic loading, $k_h = 0$), (ii) $k_h = 0.15$, and (iii) $k_h = 0.30$. The effect of slope saturation is captured in Fig. 5 by varying

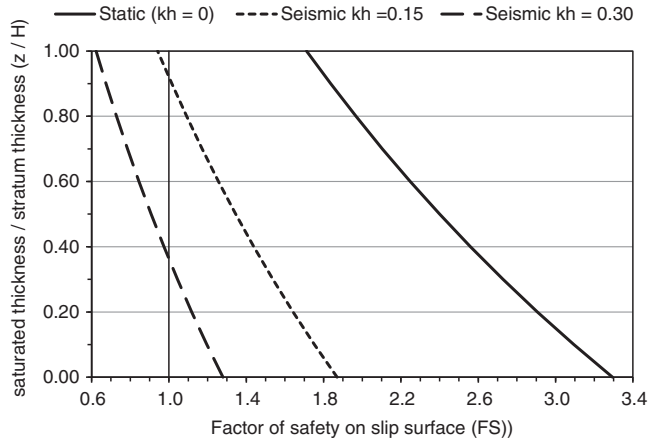

Fig. 5. Factor of safety for long slope with phreatic surface parallel to the slope surface as a function of the saturation ratio (z/H) and seismic loading; $c' = 0$, $\phi' = 35°$, $H = 3$ m, $\gamma_{sat} = 20.42$ kN/m^3, γ (dry) $= 15.71$ kN/m^3, slope angle $\beta = 12°$.

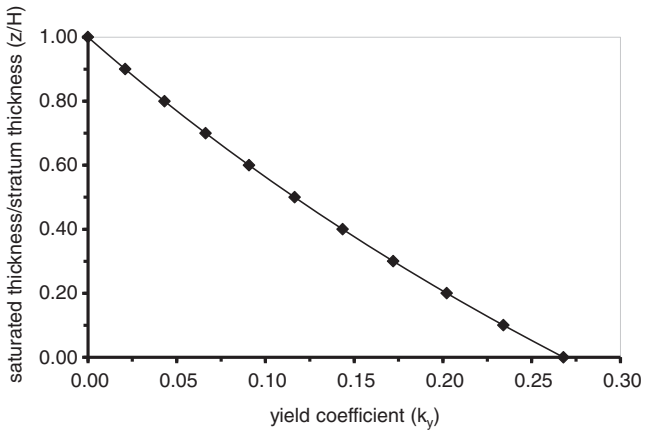

Fig. 7. The yield coefficient as a function of the saturation ratio (z/H). The slope parameters are identical to those used to prepare Figs. 5 and 6, except that the slope angle $\beta = 20°$.

the saturation thickness z from 0 (dry slope case) to $z = H$ (completely saturated slope).

It is seen in Fig. 5 the strong effect that saturation has on slope stability. The factor of safety is nearly halved as the slope soil changes from dry to completely saturated for all cases of seismic loading. The case $k_h = 0.15$ starts with a stable situation when $z/H = 0$ and becomes unstable ($FS = 1$) when $z/H = 0.90$. The case $k_h = 0.30$ is stable when dry and becomes stable when $z/H = 0.35$.

Fig. 6 continues the example presented in Fig. 5 highlighting the effect of the slope angle β on slope stability. Notice in Fig. 6 that doubling the slope angle from 12° (used to prepare Fig. 5) to 24° renders the slope marginally stable even when it is dry. A saturation ratio $z/H = 0.10$ renders the slope unstable when the lateral seismic coefficient $k_h = 0.15$.

Fig. 7 shows the role of slope saturation on the yield coefficient k_y. The slope parameters are identical to those used to prepare Figs. 5 and 6, except that the slope angle $\beta = 20°$. Fig. 7 portrays the strong effect that slope saturation has on the yield coefficient, and, thus, on slope deformation (to be elaborated upon below). In fact, full slope saturation ($z/H = 1$) produces a slope with $k_y = 0$, which induces slope deformation by any level of seismic shaking.

Fig. 8 depicts the impact that slope saturation and the maximal horizontal acceleration in bedrock (MHA_r) has on slope deformation as measured by the median lateral displacement (u) defined by Stewart et al. (2003). The slope parameters are identical to those used to prepare Fig. 7. Notice in Fig. 8 that large slope deformations occur when $z/H = 1$, which, as shown in Fig. 7, is associated with a yield coefficient = 0.

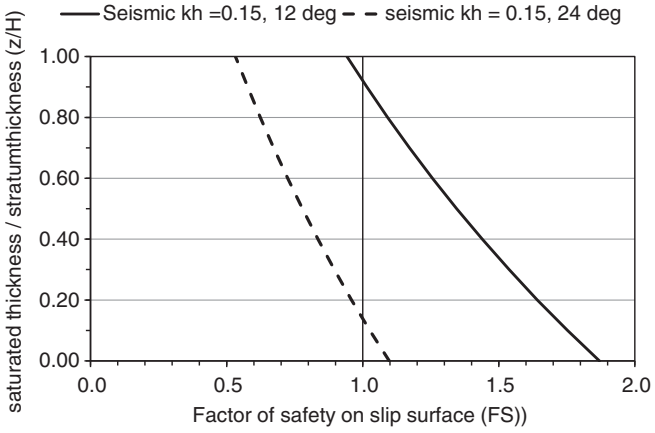

Fig. 6. Factor of safety as a function of the saturation ratio (z/H) and slope angle ($\beta = 12°$, 24°). Other parameters identical to those used to prepare Fig. 5.

The next example, illustrated in Fig. 9, involves slope stability analysis when the phreatic surface emerges from the slope surface. See Fig. 4 describing the geometry of a long slope with emerging phreatic surface. The slope parameters are slope angle $\beta = 12°$, $\phi' = 35°$, $c' = 0$, $\gamma_{sat} = 20.42$ kN/m^3, $\gamma = 15.71$ kN/m^3, angle of the phreatic surface $\varphi = 6°$, and slope thickness $H = 3$ m. The static loading case ($k_h = 0$) produces a factor of safety equal to 1.67 in Fig. 9.

The factor of safety for dry slope in Fig. 9 when the seismic load is nil ($k_h = 0$) is almost twice ($FS = 3.29$) that associated with static loading when there is an emerging phreatic surface ($FS = 1.67$). The slope becomes unstable under seismic loading when $k_h = 0.125$, whereas the slope remains stable for seismic coefficient as high as 0.30 when the slope is dry.

Fig. 10 illustrates the variation of the factor of safety and the yield coefficient under undrained loading due to changing phreatic surface, applying total-stress analysis with $\phi_T = 0$. The phreatic surface is parallel to the slope surface. The parameters are: $s_q = 30$ kPa (dynamic shear strength), $k_h = 0.15$, $H = 3$ m, $\gamma_{sat} = 20.42$ kN/m^3, γ (dry) $= 15.71$ kN/m^3, and slope angle $\beta = 26.6°$ (2H:1V).

It is seen in Fig. 10 that the factor of safety is reduced from a stable condition under dry condition ($z/H = 0$) to unstable when z/H equals or exceeds 0.70. In this case, the reduction in the factor of safety is entirely due to changes in the weight of the sliding mass as the phreatic surface rises, since the pore pressure on the slip surface does not play a role in the undrained loading case. Notice in Fig. 10, also, that the yield coefficient is reduced threefold from about 0.30 when the slope

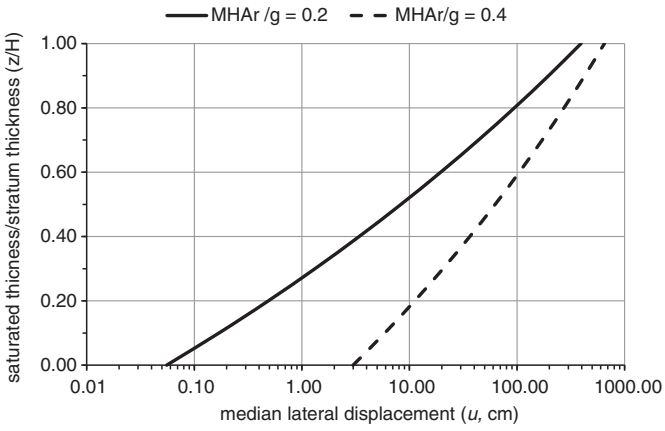

Fig. 8. Slope deformation as function of the saturation ratio (z/H) for two levels of maximum horizontal acceleration on bedrock. The slope parameters are identical to those used to prepare Fig. 7.

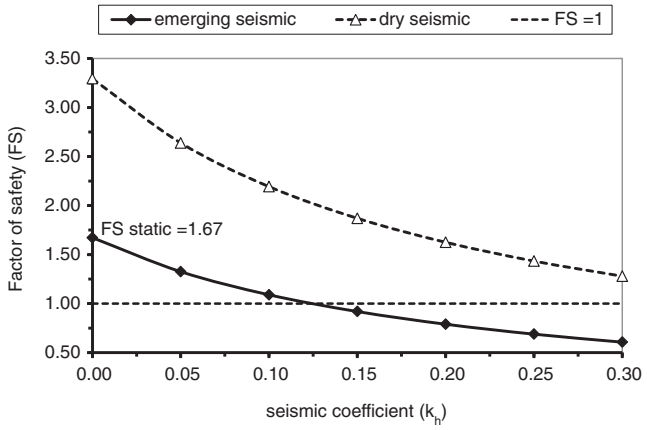

Fig. 9. Slope stability results for long slope with emerging phreatic surface. Slope angle $\beta = 12°$, $\phi' = 35°$, $c' = 0$, $\gamma_{sat} = 20.42$ kN/m^3, $\gamma = 15.71$ kN/m^3, $\varphi = 6°$, slope thickness $H = 3$ m.

is dry to about 0.10 when the slope is fully saturated. This implies increasing deformation of the slope with rising saturation conditions.

Fig. 11 illustrates the variation of the factor of safety and the yield coefficient under undrained loading due to changing slope angle applying total-stress analysis with $\phi_T = 0$. The phreatic surface emerges from the slope (see Fig. 4). The parameters used to calculate the FS in Fig. 11 are: $s_q = 30$ kPa (dynamic shear strength), $k_h = 0.15$, $H = 3$ m, $\gamma_{sat} = 20.42$ kN/m^3, and variable slope angle β. The calculation of the yield coefficient was based on $s_q = 30$ kPa, $H = 3$ m, $\gamma_{sat} = 20.42$ kN/m^3, and variable slope angle β.

Fig. 11 clearly demonstrates that the factor of safety and the yield coefficient decrease with increasing slope angle, other variables held constant. The factor of safety equals one when the slope angle is 23.3°, in which case the yield coefficient equals 0.15. Fig. 11 also shows that the yield coefficient equals zero when the slope angle is 39°. This means that for an angle of 39° the slope is statically unstable: any seismic ground motion would produce downslope displacement.

6.2. Clay softening in long slopes with parallel phreatic surface

A long slope with parallel phreatic surface provides the geometry used in this example. See Fig. 3 for the pertinent geometry. The parameters used are: (static) undrained shear strength $s_u = 30$ kPa, slope angle $\beta = 28°$, $\gamma = 15.71$ kPa; $\gamma_{sat} = 20.42$ kPa; $H = 3.0$ m; moment

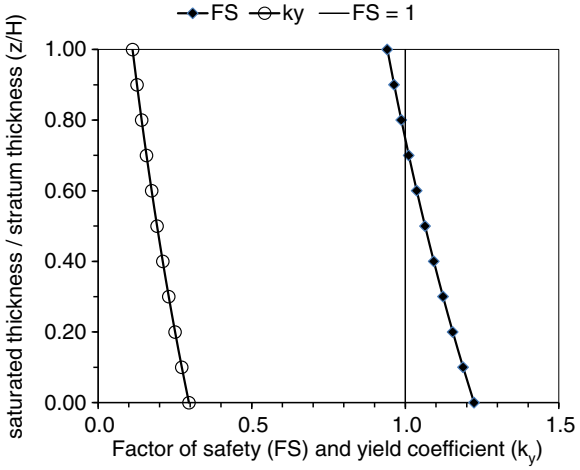

Fig. 10. The factor of safety (FS) and yield coefficient for undrained loading, total-stress analysis with $\phi_T = 0$. Phreatic surface parallel to the slope surface. Total stress analysis with $\phi_T = 0$.

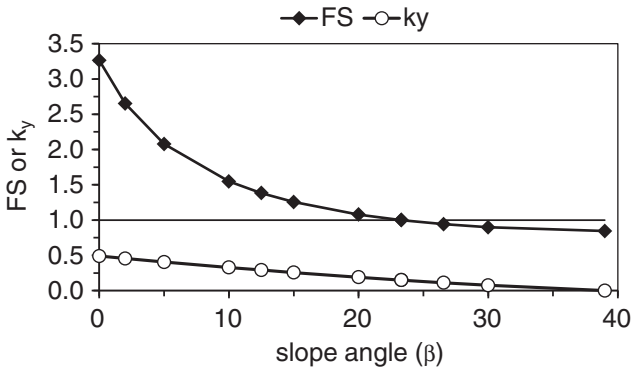

Fig. 11. Effect of the slope angle on the factor of safety (FS) and yield coefficient (k_y), long slope with emerging phreatic surface. Total stress analysis with $\phi_T = 0$.

magnitude of earthquake $M = 7.5$; maximum horizontal ground acceleration ratio $MHA/g = 0.16$, and clay overconsolidation ratio $OCR = 1$. The theoretical model for clay softening assessment is given by Eq. (7), which defines the factor of safety against clay softening. Eq. (7) involves the static stress factor $K_{\alpha,CS}$ that accounts for the effect of static shear stress on clay softening. $K_{\alpha,CS}$ depends on the vertical stress on the slip surface, which, in turn, depends on the saturation ratio z/H. It is through these series of relations that slope saturation affects clay softening. The formula for the static stress factor at a depth z on the slip surface is (Idriss and Boulanger, 2008):

$$K_\alpha(z) = 1.344 - \frac{0.344}{\left(1 - \frac{\tau_{stat}(z)}{s_u(z)}\right)^{0.638}} \tag{33}$$

The static shear stress on the slip surface of a long slope with parallel phreatic surface, see Fig. 3, equals:

$$\tau_{stat} = \gamma_{avg}\, H \cos\beta \sin\beta \tag{34}$$

where the average unit weight is equal to $\gamma_{avg} = (\gamma(H - z) + \gamma_{sat}\, z)/H$.

Fig. 12 depicts the effect that the slope saturation ratio has on clay softening, where it is shown that the monotonic increase of the saturation ratio decreases monotonically the factor of safety against clay softening presented in Eq. (7).

It is seen in Fig. 12 that the factor of safety against clay softening falls below 1 when the saturation ratio z/H exceeds about 0.95. At that juncture, the clay would undergo large deformations as a result of a decline in its dynamic shear strength.

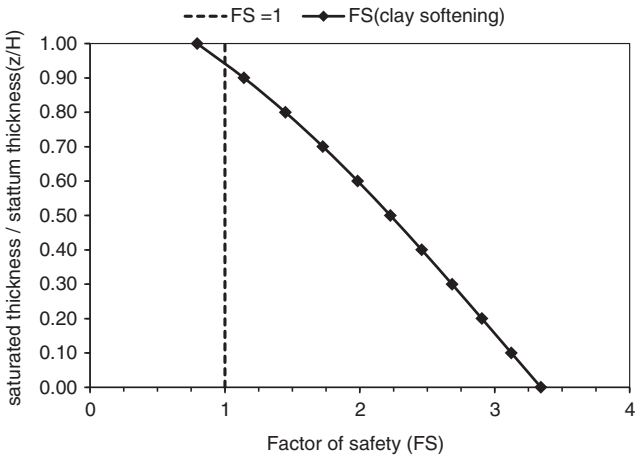

Fig. 12. Dependence of the factor of safety against clay softening on slope saturation.

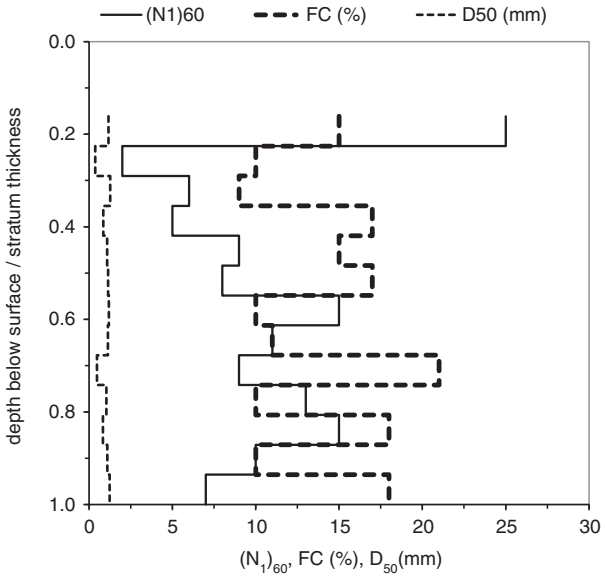

Fig. 13. Normalized SPT $(N_1)_{60}$, fines content (FC), mean diameter D_{50} at borehole 1C, Port Island, Japan.
Data from Youd et al., 2002.

6.3. The effect of groundwater on lateral spread displacement calculated using regression formula

This example uses data from Youd et al. (2002) collected at borehole 1C in Port Island, Japan, following the magnitude 6.9 Kobe earthquake of 1995 to calculate the lateral spread displacement using Eqs. (20) and (21). Fig. 13 outlines a soil profile of the normalized SPT resistance $(N_1)_{60}$, fines content (FC), mean diameter D_{50} at borehole 1C. The total thickness of the soil section is $H = 15.5$ m. The distance $R = 5$ km (assumed) and the slope $S = 1\%$ (assumed).

Fig. 14 graphs the calculated lateral spread displacement corresponding to the data shown in Fig. 13. The lateral spread displacement is graphed in Fig. 14 as a function of the depth to the phreatic surface.

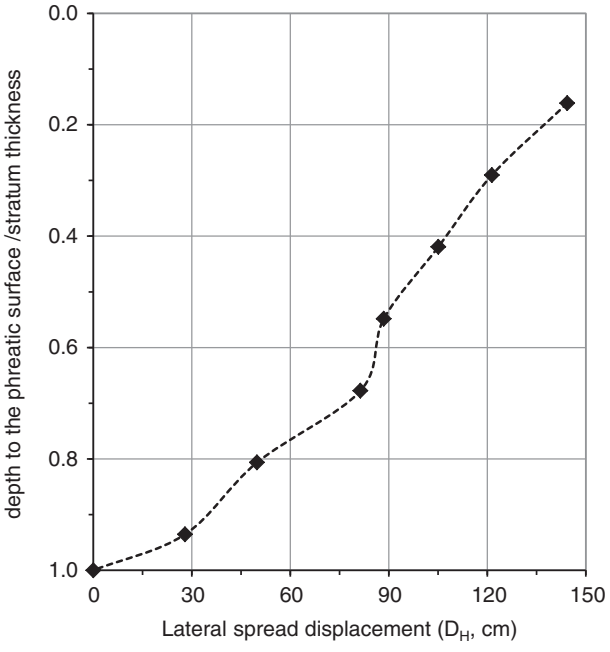

Fig. 14. Lateral spread displacement as a function of the depth to the phreatic surface.

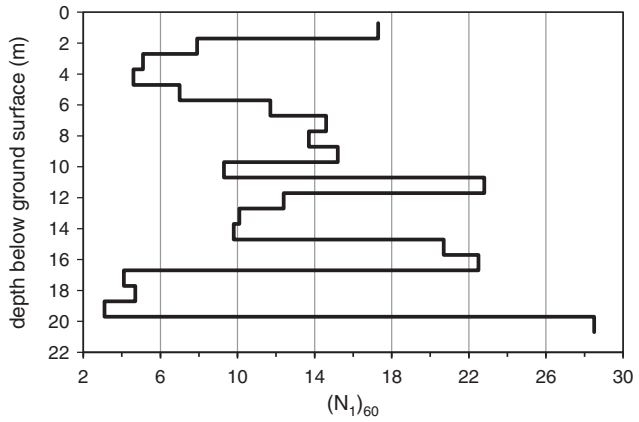

Fig. 15. Profile of normalized SPT resistance for a site affected by the Niigata earthquake.

It is evident from Fig. 14 the monotonic increase of the lateral deformation with rising phreatic surface.

6.4. The effect of groundwater on the lateral and vertical deformation of liquefied sand

The last example uses data for a site affected by the 1964, magnitude 7.5, Niigata earthquake, Japan, presented by Kramer (1996). The dry unit weight $\gamma = 18.384$ kN/m^3, $\gamma_{sat} = 21.386$ kN/m^3, $MHA = 0.16$ g, gently sloping terrain. The profile of the normalized SPT resistance $(N_1)_{60}$ at the site is depicted in Fig. 15.

Notice in Fig. 15 very loose layers between 2.5 and 4.5 m and between 16.5 and 19.5 m below ground surface.

Fig. 16 shows the calculated factor of safety against liquefaction (see Eq. (5)) corresponding to a high phreatic surface (1.2 m below the ground surface) and to a deep phreatic surface (11.2 m below the ground surface). It is seen in Fig. 16 that the majority of the soil profile is liquefied when the phreatic surface is high. When the phreatic surface is deep, on the other hand, it is seen that only the very loose layers between 16.5 and 19.5 m liquefy.

The factor of safety against liquefaction as a function of depth for various elevations of the phreatic surface was calculated and used to calculate the lateral displacement index (LDI, Eq. (30)) and vertical reconsolidation (S_v, Eq. (32)) for variable groundwater conditions. The results are shown on Fig. 17. Notice in Fig. 17 that the lateral and vertical deformations increase with decreasing depth to the phreatic surface. In

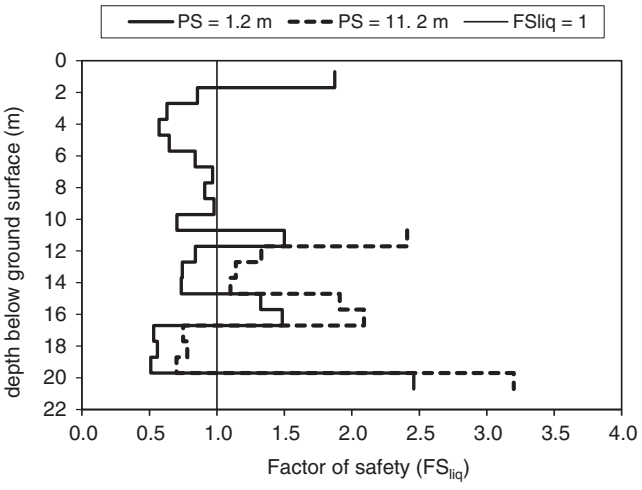

Fig. 16. Factor of safety against liquefaction for two positions of the phreatic surface (PS) at site affected by the 19654 Niigata earthquake.

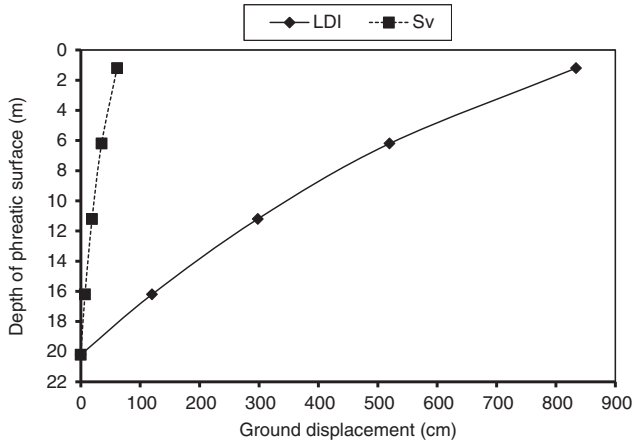

Fig. 17. Lateral displacement index (LDI) and vertical reconsolidation (S_v) as function the depth of the phreatic surface for site affected by 1964 Niigata earthquake.

this case, the lateral displacement index is about one order of magnitude larger that the vertical reconsolidation.

7. Conclusion

This paper has provided a set of results for the factor of safety and the yield coefficient concerning the stability of common slope configurations. The innovation of the paper is several-fold: (1) development of closed-form equations for the factor of safety and the yield coefficient considering the simultaneous actions of seismic forces and variable groundwater conditions, (2) consideration of the principal modes of drainage during loading, that is, the undrained and drained conditions, highlighting the roles of total stress and effective stress analyses, (3) incorporation in the slope stability and deformation analysis of new advances in geotechnical earthquake engineering and seismic engineering geology concerning the seismic coefficient, liquefaction, and clay softening.

This paper has demonstrated through numerous examples how its results can be applied in the screening analysis of seismic slope stability. One common thread of the findings of this paper is the importance of controlling the elevation and shape of the phreatic surface to diminish the threats of slope failure, liquefaction, clay softening, and slope deformation. This paper's results provide a foundation to assist in designs of slope modification for groundwater control and to protect against earthquakes.

Acknowledgment

Dr. Pamela G. Emch provided helpful editorial comments that improved the presentation of this work.

References

Anderson, S.A., Sitar, N., 1995. Analysis of rainfall-induced debris flows. J. Geotech. Eng. 121 (7), 544–552.
Bishop, A.W., 1955. The use of the slip circle in the stability analysis of slopes. Geotechnique 5, 7–17.
Bishop, A.W., Morgenstern, N.R., 1960. Stability coefficients for earth slopes. Geotechnique 10, 129–147.
Blake, T.F., D'Antonio, R., Earnest, J., Gharib, F., Hollingsworth, R.A., Horsman, L., Hsu, D., Kupferman, S., Masuda, R., Pradel, D., Real, C., Reeder, W., Sathialingam, N., Simantob, E., Stewart, J.P., 2002. Recommended Procedures for Implementation of DMG Special Publication 117 Guidelines for Analyzing and Mitigating Landslide Hazards in California. Southern California Earthquake Center, University of Southern California, Los Angeles, California.
Brien, D.L., Reid, M.E., 2008. Assessing deep-seated landslide susceptibility using 3-D groundwater and slope stability analyses, southwestern Seattle, Washington. Geol. Soc. Am. Rev. Eng. Geol. XX, 83–101.
California Geological Survey, 2008. Guidelines for evaluating and mitigating seismic hazards in California. Special Publication 117A, Sacramento, California.
Cedegreen, H.R., 1989. Seepage, Drainage, and Flow Nets. John Wiley & Sons, New York.
Chacón, J., Irigaray, C., Fernández, T., El Hamdouni, R., 2006. Engineering geology maps: landslides and geographical information systems. Bull. Eng. Geol. Environ. 65, 341–411.
Cruden, D.M., Varnes, D.J., 1996. Landslide types and processes. In: Turner, A.K., Schuster, R.L. (Eds.), Landslides: Investigations and Mitigation. Transportation Research Board, Special Report 247. National Academy Press, Washington D.C., pp. 36–75.
Duncan, J.M., 1996. State of the art: limit equilibrium and finite-element analysis of slopes. J. Geotech. Eng. 122 (7), 577–596.
Duncan, J.M., Wright, S.G., 2005. Soil Strength and Slope Stability. John Wiley & Sons, New Jersey.
Evans, S.G., Bent, A.L., 2004. The Las Colinas landslide, Santa Tecla, a highly-destructive flowslide triggered by the January 13, 2001, El Salvador earthquake. Geol. Soc. Am. Spec. Pap. 375, 25–37.
Gray, D.H., Megahan, W.F., 1981. Forest vegetation removal and slope stability in the Idaho Batholith. Research Paper INT-271. Intermountain Range and Experiment Station, U.S. Forest Service, Boise, Idaho.
Griffiths, D.V., Lane, P.A., 1999. Slope stability analysis by finite elements. Geotechnique 49 (3), 387–403.
Griffiths, D.V., Marquez, R.M., 2007. Three-dimensional slope stability by elasto-plastic finite elements. Geotechnique 57 (6), 537–546.
Harp, E.L., Keefer, D.K., Sato, H.P., Yagi, H., 2011. Landslide inventories: the essential part of seismic landslide hazard analysis. Eng. Geol. 122, 9–21.
Hynes-Griffin, M.E., Franklin, A.G., 1984. Rationalizing the seismic coefficient method. Miscellaneous Paper GL-84-13. Waterways Experiment Station, United States Army Corps of Engineers, Vicksburg, Mississippi.
Idriss, I.M., Boulanger, R.W., 2008. Soil Liquefaction During Earthquakes. Earthquake Engineering Research Institute MNO-12, Oakland California.
Iverson, R.M., 2000. Landslide triggering by rain infiltration. Water Resour. Res. 36, 1897–1910.
Jibson, R.W., 2011. Methods for assessing the stability of slopes during earthquakes — a retrospective. Eng. Geol. 122, 43–50.
Jibson, R.W., Keefer, D.K., 1993. Analysis of the seismic origin of earthquakes: examples from the New Madrid seismic zone. Geol. Soc. Am. Bull. 105, 521–536.
Keefer, D.K., 1984. Landslides caused by earthquakes. Geol. Soc. Am. Bull. 95, 406–421.
Keller, E.A., Loáiciga, H.A., 1993. Fluid-pressure induced seismicity at regional scales. Geophys. Res. Lett. 20 (16), 1683–1686.
Koerner, R.M., 2012. 6th ed. Designing With Geosynthetics vol. 2. Xilibris Corporation, Philadelphia.
Kramer, S.L., 1996. Geotechnical Earthquake Engineering. Prentice Hall, New Jersey.
Lambe, T.W., Whitman, R.V., 1979. Soil Mechanics SI Version. John Wiley & Sons, New York.
Loáiciga, H.A., 2005. Steady-state phreatic surfaces in sloping aquifers. Water Resour. Res. 41, W08402. http://dx.doi.org/10.1029/2004WR003861.
Maksidi, F.I., Seed, H.B., 1978. Simplified procedure for estimating dam and embankment-induced deformations. Journal of Geotechnical Engineering 104 (7), 849–867 SS.
Marcuson III, W.F., 1981. Earth Dams and Stability of Slopes Under Dynamic Loads. Proceedings of the Intl. Conference on Recent Advances in Geotechnical Earthquake Engineering and Soil Dynamics. St. Louis, Missouri vol. 3, p. 1175.
Miller, D.J., Sias, J., 1998. Deciphering large landslides linking hydrological, groundwater, and slope stability models through GIS. Hydrol. Process. 12, 923–941.
Mogami, T., Kubu, K., 1953. The behavior of soil during vibration. Proceedings of the 3rd Intl. Conference on Soil Mechanics and Foundation Engineering 1. Soil Mechanics Foundation, Zurich, pp. 152–166.
Newmark, N.M., 1965. Effects of earthquakes on dams and embankments. Geotechnique 15 (2), 139–160.
Noda, S., Uwabe, T., Chiba, T., 1975. Relation between seismic coefficient and ground acceleration for gravity quaywall. Rep. Port Harbor Res. Inst. 14 (4) (in Japanese).
Petersen, M.D., Frankel, A.D., Harmsen, S.C., Mueller, C.S., Halle, K.M., Wheeler, R.L., Wesson, R.L., Zeng, Y., Boyd, O.S., Perkins, D.M., Luco, N., Field, E.H., Wills, C.J., Rukstales, K.S., 2008. Documentation for the 2008 Update of the United States Seismic Hazard Maps. United States Geological Survey Open-File Report 2008-1128, Reston, Virginia.
Schulz, W.H., Galloway, S.L., Higgins, J.D., 2012. Evidence for earthquake triggering of large landslides in coastal Oregon, USA. Geomorphology 141–142, 88–98.
Seed, H.B., 1966. A method for earthquake-resistant design of earth dams. J. Soil Mech. Found. Eng. 92, 13–41.
Seed, H.B., 1967. Slope stability during earthquakes. J. Soil Mech. Found. Eng. 93, 299–323.
Seed, H.B., 1968. Landslides during earthquakes due to soil liquefaction. J. Soil Mech. Found. Eng. 94, 1053–1122.
Seed, H.B., 1979. Considerations in the earthquake-resistant design of earth and rockfill dams. Geotechnique 29 (3), 215–263.
Seed, R.B., Harder, L.F., 1990. SPT-based analysis of cyclic pore pressure generation and undrained residual strength. In: Duncan, J.M. (Ed.), Proceedings, H. Bolton Seed Memorial Symposium vol. 2. University of California, Berkeley, California, pp. 351–376.
Seed, H.B., Idriss, I.M., 1971. Simplified procedure for evaluating liquefaction potential. J. Geotech. Eng. 97 (9), 1249–1273.
Stark, T.D., Mesri, G., 1992. Undrained shear strength of sands for stability analysis. J. Geotech. Eng. 118 (11), 1727–1747.
Stark, T.D., Poeppel, A.R., 1994. Landfill liner interface strengths from torsional ring shear tests. J. Geotech. Eng. 120 (3), 597–615.
Stewart, J.P., Blake, T.F., Hollingsworth, R.A., 2003. A screen analysis procedure for seismic slope stability. Earthquake Spectra 19 (3), 697–712.
Swanston, D.N., Lienkaemper, G.W., Mersereau, R.C., Levno, A.B., 1988. Timber harvest and progressive deformation of slopes in southwestern Oregon. Bull. Assoc. Eng. Geol. 25, 371–381.

Terzaghi, K., 1950. Mechanisms of landslides. Engineering Geology (Berkeley) Volume. Geological Society of America, Denver.
Tokimatsu, K., Bolton Seed, H., 1987. Evaluation of settlements in sands due to earthquake shaking. J. Geotech. Eng. 113 (8), 861–878.
Towhata, I., 2008. Geotechnical Earthquake Engineering. Springer Verlag, Berlin.
Wang, G., Sassa, K., 2001. Factors affecting rainfall-induced flowslides in laboratory flumes tests. Geotechnique 51 (7), 587–599.
Yoshimine, M., Nishizaki, H., Amano, K., Hosono, Y., 2006. Flow deformation of liquefied sand under constant shear load and its application to of flow slide in infinite slope. Soil Dyn. Earthq. Eng. 26 (1), 253–254.
Youd, T.L., Idriss, I.M., Andrus, R.D., Arango, I., Castro, G., Christian, J.T., Dobry, R., Liam Finn, W.D., Harder Jr., R.F., Hynes, M.E., Ishihara, K., Koester, J.P., Liao, S.S.C., Marcuson III, W.F., Martin, G.R., Mitchell, J.K., Moriwaki, Y., Power, M.S., Robertson, P.K., Seed, R.B., Stokoe II, K.H., 2001. Liquefaction resistance of soils: summary report from the 1996 NCEER and 1998 NCEER/NSF workshops on evaluation of liquefaction resistance of soils. J. Geotech. Geoenviron. Eng. 127 (10), 817–833.
Youd, T.L., Hansen, C.M., Bartlett, S.F., 2002. Revised multilinear regression equations for prediction of lateral spread displacement. Journal of Geotechnical and Geoenvironmental Engineering 128 (12), 1007–1017.
Zhang, G., Robertson, P.K., Brachman, R.W.I., 2004. Estimating liquefaction-induced lateral displacements using standard penetration test or cone penetration test. J. Geotech. Geoenviron. 130 (8), 861–871.